# Millimeter Wave Energy Harvesting

**3 authors:**

Talha Ahmed Khan
University of Texas at Austin
**24** PUBLICATIONS   **648** CITATIONS

Ahmed Alkhateeb
Arizona State University
**236** PUBLICATIONS   **21,404** CITATIONS

Robert W. Heath
University of California, San Diego
**1,009** PUBLICATIONS   **84,939** CITATIONS

# Millimeter Wave Energy Harvesting

Talha Ahmed Khan, Ahmed Alkhateeb, and Robert W. Heath Jr.

**Abstract**

The millimeter wave (mmWave) band, which is a prime candidate for 5G cellular networks, seems attractive for wireless energy harvesting. This is because it will feature large antenna arrays as well as extremely dense basestation deployments. The viability of mmWave for energy harvesting though is unclear, due to the differences in propagation characteristics such as extreme sensitivity to building blockages. This paper considers a scenario where low-power devices extract energy and/or information from the incident mmWave signals. Leveraging tools from stochastic geometry, closed-form expressions are derived to characterize the energy coverage probability, the average harvested power, and the overall (energy-and-information) coverage probability at a typical wireless-powered device in terms of important parameters, such as the cellular network density, the antenna geometry parameters, and the channel parameters. Numerical results reveal several network and device level design insights. For example, at the basestations, the antenna geometry parameters such as beamwidth can be optimized to maximize the network-wide energy coverage for a given user population. At the device level, the overall performance can be substantially improved by optimally splitting the received signal for energy and information extraction, and by deploying multi-antenna arrays. For the latter, an efficient low-power multi-antenna mmWave receiver architecture is proposed for simultaneous energy and information transfer. Overall, simulation results suggest that mmWave energy harvesting generally provides a substantial performance gain over lower frequency solutions.

## I. Introduction

Millimeter wave (mmWave) communications is a key candidate technology for future 5G cellular networks. This is mainly due to the availability of large spectrum resources at higher frequencies, which leads to much higher data rates. Recent research suggests that mmWave

systems will typically feature (i) large-dimensional antenna arrays with directional beamforming at the transmitter/receiver—which is motivated by the small wavelength that allows packing a large number of antenna elements into small form-factors; and (ii) a dense deployment of basestations (BSs) to ensure comparable coverage to ultra high frequency (UHF) networks [1], [2]. These mmWave design features are also attractive for RF (radio frequency) energy harvesting where a harvesting device may extract energy from the incident RF signals [3]. This could potentially power the massive number of low-power wireless devices in future paradigms such as the Internet of Things [4]. The signal propagation at mmWave frequencies, however, suffers from poor penetration and diffraction characteristics, making it sensitive to blockage by buildings [2], [5]. It is, therefore, unclear if mmWave cellular networks will be more favorable for RF energy harvesting compared to the conventional (below 6 GHz) frequencies. Further, the network level design principles for mmWave energy harvesting systems are not well understood. This motivates a network view on energy harvesting in a mmWave cellular network.

## A. Contributions

In this paper, we provide a tractable framework to characterize the performance of wireless energy and information transfer aided by a large-scale mmWave cellular network. Our analysis accounts for the key distinguishing features of mmWave systems, namely the sensitivity to blockage and the use of potentially large antenna arrays at the transmitter/receiver. We first consider mmWave energy harvesting, where devices only extract energy from the incident mmWave signals. Our analysis models two operating scenarios, one where devices have their beams aligned to that of a mmWave BS, and the other where no such beam alignment is assumed. For both operating modes, we derive simple analytical expressions for metrics such as the energy coverage probability and the average harvested power using tools from stochastic geometry. We then extend the analysis to characterize the overall (energy-and-information) coverage probability for the general case where a device extracts both energy and information from the mmWave signals.

To get design insights, we examine the network level performance trends in terms of key parameters such as the mmWave network density and the antenna geometry parameters for both operating modes of the energy harvesting devices. Numerical results suggest that narrower antenna beams should be preferred when the users are aligned with a BS, whereas wider beams

are favorable when no beam alignment is assumed. Our findings also suggest that there typically exists an optimum transmit antenna beamwidth that maximizes the network-wide energy coverage for a given user population. This implies that the mmWave BSs will need to adapt the antenna beam patterns depending on the fraction of the users operating in each mode.

Similar to the BS-related parameters, we also investigate the role of device-related parameters on system performance. For example, the overall (energy-and-information) coverage probability can be substantially improved by optimizing over a design parameter (power splitting ratio) to optimally portion the received signal between the energy harvesting and the information decoding modules. Another important design feature at the user is the receive antenna array. Similar to the BSs, the mmWave users can, in principle, benefit from using large antenna arrays. For low-power energy harvesting devices, however, the associated antenna circuity could increase the power consumption, offsetting the potential gains of large antenna arrays. To leverage multiple antennas at the receiver without resorting to power-hungry circuit components, we propose a simple switch-based receiver architecture for simultaneous energy and information transfer. Simulation results reveal that the proposed low-power solution performs reasonably well compared to more advanced but power-hungry receiver architectures.

*B. Related Work*

Wireless energy harvesting is becoming increasingly feasible due to the reduction in the power consumption requirements of wireless sensors and the improvements in energy harvesting technologies [6]–[9]. This has also led to considerable research in advancing the theoretical understanding of wireless powered systems (see [3], [10] for a comprehensive overview). For example, wireless energy and information transfer has been studied for different information-theoretic setups such as a broadcast channel [11], a fading channel [12], and an interference channel [13]. Many of these papers highlight the fundamental trade-off between energy and information transfer efficiency and characterize the achievable rate-energy regions for different practical receiver architectures [10].

Wireless energy and/or information transfer in large-scale networks has also been investigated [14]–[19]. In [14], the performance of ambient RF energy harvesting was characterized using tools from stochastic geometry. Using a repulsive point process to model RF transmitters, it was shown that more repulsion helps improve the performance at an energy harvester for a given trans-

mitter density. In [15], [16], cognitive radio networks were considered, and opportunistic wireless energy harvesting was proposed and analyzed. In [17], a hybrid cellular network architecture was proposed to enable wireless power transfer for mobiles. In particular, an uplink cellular network was overlaid with power beacons and trade-offs between transmit power and deployment densities were investigated under an outage constraint on the data links. A broadband wireless network with transmit beamforming was considered in [18], where optimal power control algorithms were devised for improving the throughput and power transfer efficiency. Simultaneous information and energy transfer in a relay-aided network was considered in [19]. Under a random relay selection strategy, the network-level performance was characterized in terms of the relay density and the relay selection area.

Our work differs from the prior work in that we investigate wireless energy and information transfer in a large-scale *mmWave* cellular network. Due to different physical characteristics and design features at mmWave, prior work on energy/information transfer in lower frequency networks does not directly apply to mmWave networks. In another line of work, the performance of mmWave cellular networks in terms of signal-to-interference-and-noise ratio (SINR) coverage and rate has also been analyzed using stochastic geometry [20], [21]. None of this work on mmWave networks, however, provides a performance characterization from the perspective of wireless energy and information transfer.

The paper is organized as follows. In Section II, we introduce the system model. Section III presents the analytical results for mmWave energy harvesting. The case with simultaneous information and energy transfer is treated in Section IV. We conclude the paper in Section V.

## II. SYSTEM MODEL

In this section, we introduce the network and channel models, followed by a description of the antenna model. The parameters defined in this section are summarized in Table I.

### A. Network Model

We consider a large-scale cellular network consisting of mmWave BSs and a population of wireless-powered devices (or users) that operate by extracting energy and/or information in the mmWave band. The mmWave BSs are located according to a homogeneous Poisson point process (PPP) $\Phi(\lambda)$ of density $\lambda$. The user population is drawn from another homogeneous PPP

$\Phi_u(\lambda_u)$ of density $\lambda_u$, independently of $\Phi$. In general, mmWave BSs and users may be located outdoors or indoors. Empirical evidence suggests that mmWave signals exhibit high penetration losses for many common building materials [5], [20]. Assuming the building blockages to be impenetrable, we focus on the case where the BSs and users are located outdoors. We say that a link is line-of-sight (LOS) or non-line-of-sight (NLOS) depending on whether or not it is intersected by a building blockage. Channel measurement campaigns have reported markedly different propagation characteristics for LOS/NLOS links [1], [5]. To model blockage due to buildings, we leverage the results in [22] where the buildings are drawn from a boolean stochastic point process. We define a line-of-sight (LOS) probability function $p(r) = e^{-\beta r}$ for a link of length $r$, where $\beta$ is a constant that depends on the geometry and density of the building blockage process: a BS-receiver link of length $r$ is declared LOS with a probability $p(r)$, independently of other links. While conducting stochastic geometry analysis, we will apply this result to split the BS PPP into two independent but non-homogeneous PPPs consisting of LOS and NLOS BSs.

We allow the user population to consist of two types of users, namely *connected* and *nonconnected*. A connected user is assumed to be tagged with the BS, either LOS or NLOS, that maximizes the average received power at that user. Moreover, for the connected case, we assume perfect beam alignment between a BS and its tagged user, i.e., the BS and user point their beams so as to have the maximum directivity gain. For a nonconnected user, we do not assume any prior beam alignment with a BS. This allows us to model a wide range of scenarios. For instance, due to limited resources, the mmWave network may (directly) serve only a fraction of the user population as connected users, leaving the rest in the nonconnected mode. Another interpretation could be that due to the challenges associated with channel acquisition, not all the users could be simultaneously served in the connected mode. We let $\epsilon$ be the probability that a randomly selected node is a connected user, independently of other nodes. With this assumption, we can thin the user PPP $\Phi_u$ into two independent PPPs $\Phi_{u,\text{con}}$ and $\Phi_{u,\text{ncon}}$, with respective densities $\epsilon\lambda_u$ and $(1-\epsilon)\lambda_u$. Note that an arbitrary user, either connected or nonconnected, may experience an energy outage if the received power falls short of a required threshold $\psi$. This threshold would depend on the power consumption as well as the sensitivity requirements of the harvesting circuit. We define $P_{\text{con}}(\lambda, \psi)$ to be the energy coverage probability given an outage threshold $\psi$ for a connected user, while $P_{\text{ncon}}(\lambda, \psi)$ denotes the same for the nonconnected case. With these

definitions, we can define the overall energy coverage probability $\Lambda(\epsilon, \lambda, \psi)$ of the network as

$$\Lambda(\epsilon, \lambda, \psi) = \epsilon \mathbf{P}_{\text{con}}(\lambda, \psi) + (1 - \epsilon) \mathbf{P}_{\text{ncon}}(\lambda, \psi) \tag{1}$$

where the energy coverage probability is a function of several parameters such as the BS density, the channel propagation parameters, as well as the antenna beam patterns at the transmitter/receiver. In the next section, we provide analytical expressions to compute the energy coverage probability in a mmWave network.

### B. Channel Model

We now describe the channel model for an arbitrary user without losing generality. Empirical evidence suggests that mmWave frequencies exhibit different propagation characteristics for the LOS/NLOS links [5]. While the LOS mmWave signals may propagate as if in free space, the NLOS mmWave signals typically exhibit a higher path loss exponent. We let $\alpha_{\text{L}}$ and $\alpha_{\text{N}}$ be the path loss exponents for the LOS and NLOS links respectively. We define the distance-dependent path loss for a user located a distance $r_\ell$ from the $\ell$-th BS: $g_\ell(r_\ell) = C_{\text{L}} r_\ell^{-\alpha_{\text{L}}}$ when the link is LOS, where $C_{\text{L}}$ is the path loss intercept; and $g_\ell(r_\ell) = C_{\text{N}} r_\ell^{-\alpha_{\text{N}}}$ for the NLOS case. We similarly define $h_\ell$ to be the small-scale fading coefficient corresponding to a BS $\ell \in \Phi$. Assuming independent Nakagami fading for each link, the small-scale fading power $H_\ell = |h_\ell|^2$ can be modeled as a normalized Gamma random variable, i.e., $H_\ell \sim \Gamma(N_{\text{L}}, 1/N_{\text{L}})$ when the link is LOS and $H_\ell \sim \Gamma(N_{\text{N}}, 1/N_{\text{N}})$ for the NLOS case, where the fading parameters $N_{\text{L}}$ and $N_{\text{N}}$ are assumed to be integers for simplicity.

### C. Antenna Model

To compensate for higher propagation loss, mmWave BSs will use large directional antennas arrays. We assume that the BSs and users are equipped with $N_{\text{t}}$ and $N_{\text{r}}$ antenna elements each. To simplify the analysis while capturing the key antenna characteristics, we use a sectored antenna model of Fig. 1 (except for Section VI), similar to the one considered in [20], [23]. We use $A_{M,m,\theta,\bar{\theta}}(\phi)$ to characterize the antenna beam pattern, where $\phi$ gives the angle from the boresight direction, $M$ denotes the directivity gain and $\theta$ the half power beamwidth for the main lobe, while $m$ and $\bar{\theta}$ give the corresponding parameters for the side lobe. With this notation, $A_{M_{\text{t}},m_{\text{t}},\theta_{\text{t}},\bar{\theta}_{\text{t}}}(\cdot)$ denotes the antenna beam pattern at an arbitrary BS in $\Phi$, and $A_{M_{\text{r}},m_{\text{r}},\theta_{\text{r}},\bar{\theta}_{\text{r}}}(\cdot)$ denotes the same
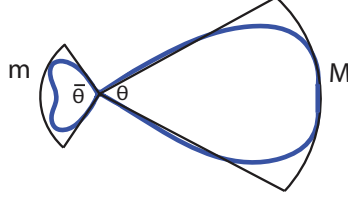
Fig. 1. Sectored antenna model. The antenna beam pattern is parameterized by the directivity gains for the main lobe ($M$) and side lobe ($m$), and the half power beamwidths for the main lobe ($\theta$) and side lobe ($\bar{\theta}$).

for an energy harvesting user in $\Phi_u$. We further define $\delta_\ell = A_{M_t, m_t, \theta_t, \bar{\theta}_t}(\phi_t^\ell) A_{M_r, m_r, \theta_r, \bar{\theta}_r}(\phi_r^\ell)$, the total directivity gain for the link between the $\ell$-th BS and the typical user; $\phi_t^\ell$ and $\phi_r^\ell$ give the angle-of-arrival and angle-of-departure of the signal.

Without any further assumptions about the beam alignment, we model the directivity gain $\delta_\ell$ as a random variable. We assume the angles $\phi_t^\ell$ and $\phi_r^\ell$ are uniformly distributed in $[0, 2\pi)$. Due to the sectored antenna model, the random variable $\delta_\ell = D_i$ with a probability $p_i$ ($i \in \{1, 2, 3, 4, 5\}$), where $D_i \in \{M_t M_r, M_t m_r, m_t M_r, m_t m_r, 0\}$ with corresponding probabilities $p_i \in \{q_t q_r, q_t \bar{q}_r, \bar{q}_t q_r, \bar{q}_t \bar{q}_r, q_o\}$; the constants $q_t = \frac{\theta_t}{2\pi}$, $\bar{q}_t = \frac{\bar{\theta}_t}{2\pi}$, $q_r = \frac{\theta_r}{2\pi}$, $\bar{q}_r = \frac{\bar{\theta}_r}{2\pi}$, and $q_o = 2 - q_t - \bar{q}_t - q_r - \bar{q}_r$. Note that $D_5 = 0$ models the extreme case where the BS and user beams have no alignment at all. Note that for the connected mode, since we assume perfect beam alignment between the typical user and its serving BS (hereby denoted by subscript 0), the directivity gain $\delta_0 = M_t M_r$ due to the sectored antenna model.

## III. MmWave with Energy Harvesting

In this section, we assume that each user is equipped with an energy harvesting circuit, and attempts to extract energy from the incident mmWave signals. No decoding of information is considered in this section. The case with simultaneous information and power transfer is treated in Section IV. We first provide analytical expressions to evaluate the energy coverage probabilities for both connected and nonconnected users. We then validate the analytical model, and conclude the section by providing network level design insights.

### A. Stochastic Geometry Analysis

We first provide some lemmas before stating the main analytical results for this section.

TABLE I
MODEL PARAMETERS

| Notation | Description |
|---|---|
| $N_t$, $N_r$ | Antenna array size at the transmitter (t) and receiver (r) |
| $M_t$, $M_r$ | Main lobe directivity gain |
| $m_t$, $m_r$ | Side lobe directivity gain |
| $\theta_t$, $\theta_r$ | Main lobe half power beamwidth |
| $\bar{\theta}_t$, $\bar{\theta}_r$ | Side lobe half power beamwidth |
| $\Phi(\lambda)$ | BS PPP with density $\lambda$ |
| $\Phi_u(\lambda_u)$ | User PPP with density $\lambda_u$ |
| $\epsilon$ | Fraction of connected users |
| $\psi$ | Energy outage threshold |
| $\Lambda(\epsilon, \lambda, \psi)$ | Energy coverage probability |
| $p(r)$ | LOS probability function |
| $\beta$ | Building blockage parameter |
| $\alpha_L$, $\alpha_N$ | LOS/NLOS path loss exponents |
| $C_L$, $C_N$ | LOS/NLOS path loss intercepts |
| $N_L$, $N_N$ | LOS/NLOS fading parameters |
| $P_t$ | Transmit power of BSs in $\Phi$ |

*Lemma 1 (From [22, Theorem 8]):* The probability density function (PDF) of the distance from an energy harvesting user to its nearest LOS BS, given that the user observes at least one LOS BS, is given by

$$\tau_L(x) = 2\pi\lambda B_L^{-1} x p(x) e^{-2\pi\lambda \int_0^x v p(v) \mathrm{d}v}, \tag{2}$$

where $x > 0$ and $B_L = 1 - e^{-2\pi\lambda \int_0^\infty v p(v) \mathrm{d}v}$ is the probability that the receiver observes at least one LOS BS. Similarly, the distance distribution of the link between the user and its nearest NLOS BS, given that the user observes at least one NLOS BS, is given by

$$\tau_N(x) = 2\pi\lambda B_N^{-1} x (1 - p(x)) e^{-2\pi\lambda \int_0^x v(1-p(v)) \mathrm{d}v}, \tag{3}$$

where $x > 0$ and $B_N = 1 - e^{-2\pi\lambda \int_0^\infty v(1-p(v)) \mathrm{d}v}$ is the probability that the user observes at least one NLOS BS.

*Lemma 2 (From [20, Lemma 2]):* Let $\varrho_L$ and $\varrho_N$ denote the probability that the energy har-

vesting user is connected to a LOS and a NLOS BS respectively, then $\varrho_\mathrm{L}$ is given by

$$\varrho_\mathrm{L} = B_\mathrm{L} \int_0^\infty e^{-2\pi\lambda \int_0^{\rho_\mathrm{L}(x)}(1-p(v))v\mathrm{d}v} \tau_\mathrm{L}(x)\,\mathrm{d}x, \tag{4}$$

where $\rho_\mathrm{L}(x) = \left(\frac{C_\mathrm{N}}{C_\mathrm{L}}\right)^{\frac{1}{\alpha_\mathrm{N}}} x^{\frac{\alpha_\mathrm{L}}{\alpha_\mathrm{N}}}$ and $\varrho_\mathrm{N} = 1 - \varrho_\mathrm{L}$.

*Lemma 3 (From [20, Lemma 3]):* Given that the energy harvesting user is connected to a LOS mmWave BS, the PDF of the link distance is given by

$$\tilde{\tau}_\mathrm{L}(x) = \frac{B_\mathrm{L}\tau_\mathrm{L}(x)}{\varrho_\mathrm{L}} e^{-2\pi\lambda \int_0^{\rho_\mathrm{L}(x)}(1-p(v))v\mathrm{d}v}, \tag{5}$$

where $x > 0$. Given that the user is connected to a NLOS mmWave BS, the PDF of the link distance is given by

$$\tilde{\tau}_\mathrm{N}(x) = \frac{B_\mathrm{N}\tau_\mathrm{N}(x)}{\varrho_\mathrm{N}} e^{-2\pi\lambda \int_0^{\rho_\mathrm{N}(x)} p(v)v\mathrm{d}v} \tag{6}$$

for $x > 0$ and $\rho_\mathrm{N}(x) = \left(\frac{C_\mathrm{L}}{C_\mathrm{N}}\right)^{\frac{1}{\alpha_\mathrm{L}}} x^{\frac{\alpha_\mathrm{N}}{\alpha_\mathrm{L}}}$.

Leveraging Slivnyak's theorem [24], we conduct the analysis at a typical energy harvesting user located at the origin without losing generality. If the BSs transmit with power $P_\mathrm{t}$, the energy harvested at a typical receiver (in unit time) can be expressed as

$$\gamma = \xi \left( \sum_{\ell \in \Phi(\lambda)} P_\mathrm{t}\delta_\ell H_\ell g_\ell(r_\ell) + \sigma^2 \right), \tag{7}$$

where $\xi \in (0,1]$ is the rectifier efficiency, and $\sigma^2 = N_o W$ gives the receiver noise power in the mmWave band where $W$ is the bandwidth, and $N_o$ is the noise power spectral density. The remaining parameters follow from Section II. Recall that given a BS $\ell \in \Phi(\lambda)$, the corresponding fading parameters will be distinct depending on whether the link is LOS or NLOS, which in turn depends on the LOS probability function (Section II-A). Further note that for the connected case, it follows from Section II-C that $\delta_0 = M_\mathrm{t}M_\mathrm{r}$ for the link from serving BS (denoted by subscript 0).

*Connected case:* The following theorem provides an analytical expression for the energy coverage probability $\mathrm{P_{con}}(\lambda,\psi) = \Pr\{\gamma > \psi\}$ at a connected user, where the random variable $\gamma$ is given in (7) and $\psi$ is the energy outage threshold. Note that $\mathrm{P_{con}}(\lambda,\psi)$ can also be interpreted as the complementary cumulative distribution function (CCDF) of the instantaneous harvested

energy.

*Theorem 1:* In a mmWave network with density $\lambda$, the energy coverage probability $P_{\text{con}}(\lambda, \psi)$ for the connected case given an energy outage threshold $\psi$ can be evaluated as

$$P_{\text{con}}(\lambda, \psi) = P_{\text{con,L}}\left(\lambda, \hat{\psi}\right) \varrho_{\text{L}} + P_{\text{con,N}}\left(\lambda, \hat{\psi}\right) \varrho_{\text{N}}, \tag{8}$$

where $\hat{\psi} = \frac{\psi}{\xi} - \sigma^2$, $\varrho_{\text{L}} = 1 - \varrho_{\text{N}}$ is given in Lemma 2, while $P_{\text{con,L}}(\cdot)$ and $P_{\text{con,N}}(\cdot)$ are the conditional energy coverage probabilities given the serving BS is LOS or NLOS. These terms can be tightly approximated as

$$P_{\text{con,L}}(\lambda, \psi) \approx \sum_{k=0}^{N} (-1)^k \binom{N}{k} \int_{r_g}^{\infty} \zeta_k^{\text{L}}(r) \, e^{-\Upsilon_{k,1}(\lambda,\psi,r) - \Upsilon_{k,2}(\lambda,\psi,\rho_{\text{L}}(r))} \tilde{\tau}_{\text{L}}(r) \, \mathrm{d}r, \tag{9}$$

where $\zeta_k^{\text{L}}(x) = \left(1 + \frac{akP_{\text{t}}M_{\text{t}}M_{\text{r}}C_{\text{L}}}{\psi N_{\text{L}} x^{\alpha_{\text{L}}}}\right)^{-N_{\text{L}}}$, the approximation constant $a = N(N!)^{-\frac{1}{N}}$ where $N$ denotes the number of terms in the approximation, while $r_g$ defines the minimum link distance and is included to avoid unbounded path loss at the receiver. Similarly,

$$P_{\text{con,N}}(\lambda, \psi) \approx \sum_{k=0}^{N} (-1)^k \binom{N}{k} \int_{r_g}^{\infty} \zeta_k^{\text{N}}(r) \, e^{-\Upsilon_{k,1}(\lambda,\psi,\rho_{\text{N}}(r)) - \Upsilon_{k,2}(\lambda,\psi,r)} \tilde{\tau}_{\text{N}}(r) \, \mathrm{d}r, \tag{10}$$

where $\zeta_k^{\text{N}}(x) = \left(1 + \frac{akP_{\text{t}}M_{\text{t}}M_{\text{r}}C_{\text{N}}}{\psi N_{\text{N}} x^{\alpha_{\text{N}}}}\right)^{-N_{\text{N}}}$,

$$\Upsilon_{k,1}(\lambda, \psi, x) = 2\pi\lambda \sum_{i=1}^{4} p_i \int_x^{\infty} \left(1 - \left[1 + \frac{aP_{\text{t}}kD_iC_{\text{L}}}{\psi N_{\text{L}} t^{\alpha_{\text{L}}}}\right]^{-N_{\text{L}}}\right) p(t) t \, \mathrm{d}t, \tag{11}$$

$$\Upsilon_{k,2}(\lambda, \psi, x) = 2\pi\lambda \sum_{i=1}^{4} p_i \int_x^{\infty} \left(1 - \left[1 + \frac{aP_{\text{t}}kD_iC_{\text{N}}}{\psi N_{\text{N}} t^{\alpha_{\text{N}}}}\right]^{-N_{\text{N}}}\right) (1 - p(t)) t \, \mathrm{d}t, \tag{12}$$

and the distance distributions $\tilde{\tau}_{\text{L}}(\cdot)$ and $\tilde{\tau}_{\text{N}}(\cdot)$ follow from Lemma 3.

*Proof:* See Appendix A. ∎

Recall that $p(t) = e^{-\beta t}$ is the LOS probability function defined in Section II-A, and captures the effect of building blockages. In (9), the term $\zeta_k^{\text{L}}(\cdot)$ models the contribution from the LOS serving link, $\Upsilon_{k,1}(\cdot)$ accounts for other LOS links, and $\Upsilon_{k,2}(\cdot)$ captures the effect of the NLOS links. Similarly, $\zeta_k^{\text{N}}(\cdot)$ in (10) models the case where the serving BS is NLOS. Note that these terms

further depend on the channel propagation conditions ($\alpha_L$, $\alpha_N$, $N_L$, $N_N$, $C_L$, $C_N$), the network density $\lambda$ as well as the antenna geometry parameters (via $D_i$, $p_i$), which are summarized in Table I. Furthermore, the outage threshold $\psi$ may depend on the sensitivity of the harvesting circuit, as well as the power requirements at a particular user. The following result provides an analytical expression for the average harvested power at a connected user.

*Proposition 1:* The average harvested power for the connected case $\bar{P}_{\text{con}}$ is given by

$$\bar{P}_{\text{con}} = \xi \left( \varrho_L \bar{P}_L + \varrho_N \bar{P}_N + \sigma^2 \right), \tag{13}$$

where

$$\bar{P}_L = \int_{r_g}^{\infty} \left( P_t M_t M_r C_L r^{-\alpha_L} + \Psi_L(r) + \Psi_N(\rho_L(r)) \right) \tilde{\tau}_L(r) \, dr, \tag{14}$$

$$\bar{P}_N = \int_{r_g}^{\infty} \left( P_t M_t M_r C_N r^{-\alpha_N} + \Psi_L(\rho_N(r)) + \Psi_N(r) \right) \tilde{\tau}_N(r) \, dr, \tag{15}$$

$$\Psi_L(x) = \kappa C_L \sum_{i=1}^{4} D_i p_i \int_x^{\infty} t^{-(\alpha_L - 1)} p(t) dt, \tag{16}$$

$$\Psi_N(x) = \kappa C_N \sum_{i=1}^{4} D_i p_i \left( \frac{x^{-(\alpha_N - 2)}}{\alpha_N - 2} - \int_x^{\infty} t^{-(\alpha_N - 1)} p(t) dt \right), \tag{17}$$

and $\kappa = 2\pi\lambda P_t$.

*Proof:* See Appendix B. ∎

Note that $\bar{P}_L$ and $\bar{P}_N$ denote the average harvested power given the user is tagged to an LOS or a NLOS BS. Moreover, the average harvested power is independent of the small-scale fading parameters.

*Nonconnected case:* Having discussed the connected case, we now consider the case where a user operates in the nonconnected mode. The following theorem characterizes the energy coverage probability at a typical user for the nonconnected case.

*Theorem 2:* In a mmWave network of density $\lambda$, the energy coverage probability for the

nonconnected case $P_{\text{ncon}}(\lambda, \psi)$ given an outage threshold $\psi$ can be evaluated using

$$P_{\text{ncon}}(\lambda, \psi) \approx \sum_{k=0}^{N} (-1)^k \binom{N}{k} e^{-\Upsilon_{k,1}(\lambda, \hat{\psi}, r_g) - \Upsilon_{k,2}(\lambda, \hat{\psi}, r_g)}, \tag{18}$$

where $\Upsilon_{k,1}(\cdot)$ and $\Upsilon_{k,2}(\cdot)$ are given by (11) and (12) respectively, $\hat{\psi} = \frac{\psi}{\xi} - \sigma^2$, and $r_g$ is the minimum link distance.

*Proof:* The proof follows from that of Theorem 1 and is therefore omitted. ∎

Similar to the connected case, the energy coverage probability for this case is also a function of the propagation conditions, network density and antenna geometry parameters. The following proposition gives an analytical expression for the average harvested power for the nonconnected case.

*Proposition 2:* The average harvested power $\bar{P}_{\text{ncon}}$ for the non-connected case is given by

$$\bar{P}_{\text{ncon}} = \xi \left( \Psi_{\text{L}}(r_g) + \Psi_{\text{N}}(r_g) + \sigma^2 \right), \tag{19}$$

where $\Psi_{\text{L}}(\cdot)$ and $\Psi_{\text{N}}(\cdot)$ are given in (16) and (17) respectively.

*Proof:* The proof follows from that of Proposition 1 and is therefore omitted. ∎

The average harvested power for the nonconnected case scales linearly with the transmit power and network density. This follows from (19) since $\Psi_{\text{L}}(\cdot)$ and $\Psi_{\text{N}}(\cdot)$ scale linearly with $\kappa = 2\pi\lambda P_t$. This also suggests that increasing transmit power or density has the same effect on the average harvested power.

### B. Results and Design Insights

We first verify the accuracy of the analytical expressions provided in Section III-A using simulations. We then study how key design parameters such as the antenna beam pattern affects the energy coverage probability in purely connected ($\epsilon \to 1$) and nonconnected ($\epsilon \to 0$) networks. We also compare the performance of mmWave energy harvesting with lower frequency solutions. After developing key insights for purely connected/nonconnected scenarios, we provide energy coverage results for the general case ($0 < \epsilon < 1$), where the network serves both types of users.

*Validation:* In the following plots, the users are assumed to be equipped with a single omnidirectional receive antenna, the mmWave carrier frequency is set to 28 GHz, the blockage constant $\beta = 0.0071$ [20] and the rectifier efficiency $\xi = 1$. Fig. 2 and 3 plot the energy coverage

probability for the connected case using different model parameters. The analytical results based on Theorem 1 are obtained using $N = 5$ terms in the approximation. The simulation results are generated using Monte Carlo simulations with 10,000 runs. Similarly, using Theorem 2, Fig. 5 and 6 plot the energy coverage probability for the nonconnected case. We observe a good agreement between analytical and simulation results.

*Connected case ($\epsilon \rightarrow 1$):* In Fig. 2, we plot the energy coverage probability with three distinct transmit beam patterns for a given network density. The user is assumed to be equipped with a single omnidirectional receive antenna. We observe that the energy harvesting performance improves with narrower beams (i.e., smaller beamwidths and larger directivity gains). As the beamwidth decreases, relatively fewer beams from the neighboring BSs would be incident on a typical user. But the beams that do reach, will have larger directivity gains, which results in an overall performance improvement. This is possible due to the use of potentially large antenna arrays at the mmWave BSs. Note that this performance boost will possibly be limited due to the ensuing EIRP (equivalent isotropically radiated power) or other safety regulations on future mmWave systems [25].

For the purpose of comparison, we also plot the energy coverage probability for UHF energy harvesting under realistic assumptions. Given the current state-of-the-art [1], [26], the UHF BSs are assumed to have 8 transmit antennas each. Further, they are assumed to employ maximal ratio transmit beamforming to serve a connected user. For the channel model, we assume an IID Rayleigh fading environment and a path loss exponent of $3.6$ (no blockage is considered). The network density is set to $25$ nodes/km$^2$, which corresponds to an *average* distance of about $113$m to the closest UHF BS. The carrier frequency is set to $2.1$ GHz and the transmission bandwidth is 100 MHz. As can be seen from Fig. 2, mmWave energy harvesting could provide considerable performance gain over its lower frequency counterpart. Moreover, the anticipated dense deployments of mmWave networks would further widen this gap. This effect is illustrated in Fig. 3, where we plot the energy coverage probability for different mmWave network densities for a given transmit antenna beam pattern. In Fig. 4, we use Proposition 1 to plot the average harvested power at a typical mmWave user against the transmit array size. This figure confirms our earlier intuition that mmWave energy harvesting can benefit from (i) potentially large antenna arrays at the BSs, and (ii) high BS density, which would be the key ingredients of future mmWave cellular systems.
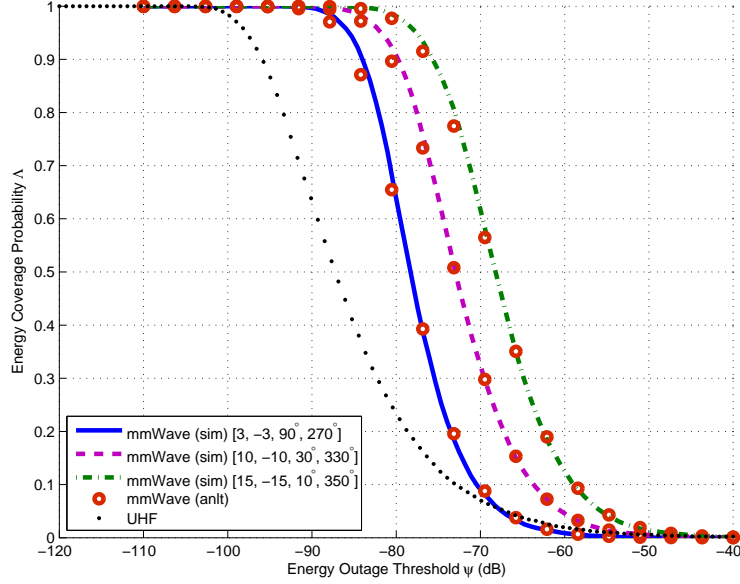
Fig. 2. Energy coverage probability $\Lambda(\epsilon, \psi, \lambda)$ for different transmit antenna beam patterns parameterized by $[M_t, m_t, \theta_t, \bar{\theta}_t]$ in a purely connected network ($\epsilon = 1$, $\lambda = 100/\text{km}^2$). The performance improves with narrower beams for this case. $P_t = 13$ dB, $W = 100$ MHz, $\alpha_L = 2$, $\alpha_N = 4$, $N_L = 2$, $N_N = 3$, and $r_g = 1$ m. There is a nice agreement between Monte Carlo simulation (sim) results and the analytical (anlt) results obtained using Theorem 1 with $N = 5$ terms.

*Nonconnected case ($\epsilon \to 0$):* We now analyze the energy harvesting performance when the harvesting devices operate in the nonconnected mode. In a stark contrast to the connected case, Fig. 5 shows that for the nonconnected case, mmWave energy harvesting could benefit from using wider beams. This is because BS connectivity is critical for the nonconnected case. With wider beams, it is more likely that a mmWave BS gets aligned with a receiver, though sacrificing the beamforming gains. Moreover, a comparison with UHF energy harvesting shows that mmWave energy harvesting gives a comparable performance to UHF solutions. Similarly, Fig. 6 plots the energy coverage probability for different deployment densities. We can observe that performance can be further improved with denser deployments, which would be a key feature in future mmWave cellular systems.

*General case ($0 < \epsilon < 1$):* Having presented the energy coverage trends for the two extreme network scenarios, we now consider the general case where the user population consists of both connected and nonconnected users. We expect this to be the likely scenario for reasons explained in the network model (Section II-A). As described in Section II-C, an antenna beam pattern can be characterized by the half power beamwidth and directivity gain for both the main and side
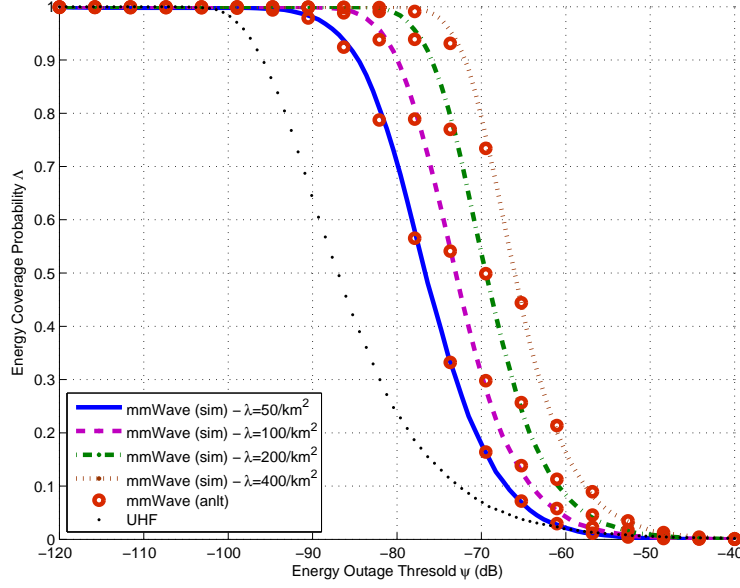
Fig. 3. Energy coverage probability $\Lambda(1, \psi, \lambda)$ for different network densities for connected users. Transmit beam pattern is fixed to $[10, -10, 30°, 330°]$. Other parameters are same as given in Fig. 2. There is a nice agreement between Monte Carlo simulation (sim) results and the analytical (anlt) results obtained using Theorem 1 with $N = 5$ terms.

lobes. By tuning these parameters, the beam pattern can be particularized to a given antenna array. As an example, we assume that uniform linear arrays (ULA) are deployed at the mmWave BSs. We use the following relations to approximate the main and side lobe beamwidths as a function of the transmit array size: $\theta_t \approx \frac{360}{\pi} \arcsin\left(\frac{0.892}{N_t}\right)$ and $\bar{\theta}_t \approx \frac{720}{\pi}\left|\arcsin\left(\frac{2}{N_t}\right)\right|$ [27]. Further, we use $M_t = 10 \log(N_t)$ and $m_t = M_t - 12$ for the directivity gains of the main and side lobes [27]. We further assume the resulting sectorized transmit beam pattern are normalized over the parameter space, i.e., $\frac{\theta_t}{2\pi} M_t + \frac{\bar{\theta}_t}{2\pi} m_t = 1$.

In Fig. 7, we plot the overall energy coverage probability $\Lambda(\epsilon, \psi, \lambda)$ against transmit array size $N_t$ for different values of parameter $\epsilon$. We find that the optimal transmit array size depends on the type of user population. For example, when $\epsilon$ is large, it is desirable to use large antenna arrays at the BSs. When $\epsilon$ is small, it is favorable to use small antenna arrays to improve the overall energy coverage probability. Depending on the network load (or the user population *mix*) captured via $\epsilon$, the energy coverage probability can be substantially improved by intelligent antenna switching schemes. Since the parameter $\epsilon$ would typically vary over large time-scales, such schemes would be practically feasible.

Having presented the energy coverage trends for mmWave energy harvesting, we now consider
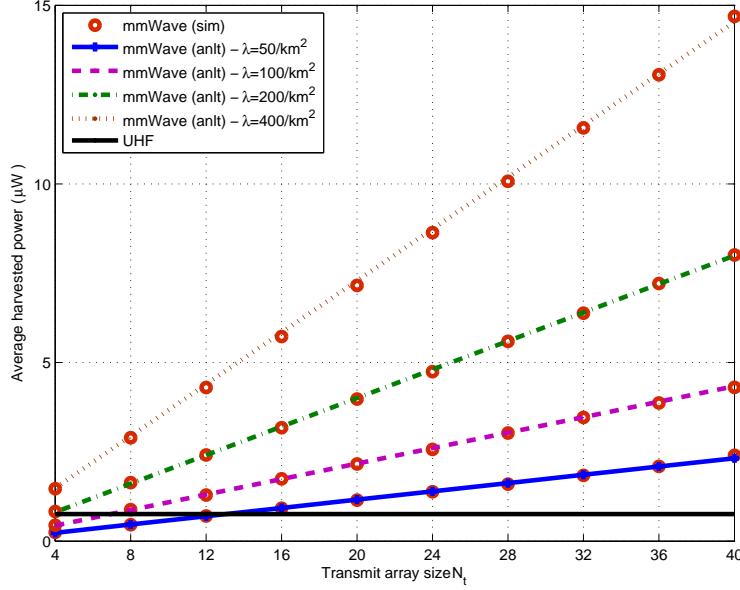
Fig. 4. The average harvested power in a connected mmWave network for different number of BS antennas $N_t$ and deployment densities $\lambda$. For comparison, a plot for a UHF system is also included. The analytical (anlt) results are based on Proposition 1. Results based on Monte Carlo simulations (sim) are also included. The transmit antenna beam patterns are calculated using the approximations used for obtaining Fig. 7. Other simulation parameters are same as used in Fig. 2.

the scenario where the user attempts to extract both power and information from the incident mmWave signals.

## IV. MmWave Simultaneous Information and Power Transfer

In this section, we consider the case where the energy harvesting device also attempts to decode information from the received signals, in what is known as simultaneous wireless information and power transfer (SWIPT). We now assume that the energy harvesting receiver is also equipped with an information decoding circuit. We focus on the case where a given user is already aligned with its serving BS, i.e., $\epsilon = 1$ for this section. Further, we consider a power splitting receiver architecture [10] where the received signal is split using factors $\sqrt{\nu}$ and $\sqrt{1-\nu}$, $\nu \in [0, 1]$. A fraction $\sqrt{1-\nu}$ of received signal is available for energy harvesting, while the remaining signal is used for information decoding. With this notation, the signal-to-interference-plus-noise ratio (SINR) at a typical receiver can be expressed as $\text{SINR} = \frac{\nu S}{\nu(I+\sigma^2)+\sigma_c^2}$, where $S = P_t M_t M_r H_0 g_0(r_0)$ denotes the useful signal power and $I = \sum_{\ell>0, \ell \in \Phi(\lambda) \backslash \mathbb{B}(r_g)} P_t \delta_\ell H_\ell g_\ell(r_\ell)$ gives the aggregate interference power from the neighboring BSs. $\sigma^2$ is the thermal noise power before splitting, while $\sigma_c^2$ captures possible signal degradation after power splitting. Similarly,
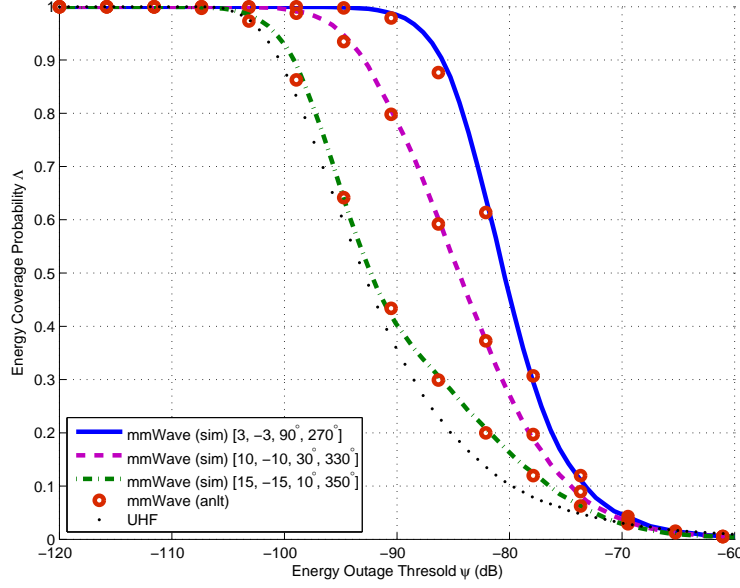
Fig. 5. Energy coverage probability $\Lambda(\epsilon, \psi, \lambda)$ for different transmit antenna beam patterns in a nonconnected network ($\epsilon = 0$, $\lambda = 100/\text{km}^2$). The performance improves with wider beams for this case. Other simulation parameters are same as given in Fig. 2. Monte Carlo simulation (sim) results validate the analytical (anlt) results obtained using Theorem 2 with $N = 5$ terms.

$\gamma = (1 - \nu)(S + I + \sigma^2)$ denotes the received signal power fed to the energy harvester. Note that a user will be in outage if the harvested energy and/or the SINR fall below their respective thresholds. We now define $P_{\text{suc}}(\lambda, T, \psi, \nu) = \Pr[\text{SINR} > T, \gamma > \psi]$ to be the probability of successful reception given the SINR outage threshold $T$, the energy outage threshold $\psi$, and the power splitting ratio $\nu$. Extending the results from the previous sections, we now provide an analytical expression to characterize the system performance with SWIPT.

### A. Stochastic Geometry Analysis

Before stating the main result of this section, we first provide a lemma for the SINR coverage probability at a mmWave receiver [20].

*Lemma 4 (From [20, Theorem 1]):* In a mmWave network of density $\lambda$, the conditional SINR coverage probability $P_{\text{cov}}(\lambda, T, \nu)$ at a SWIPT device that is not in energy outage, given an SINR outage threshold $T$ and a power splitting ratio $\nu$, is given by

$$P_{\text{cov}}(\lambda, T, \nu) = P_{\text{cov,L}}(\lambda, T, \nu)\, \varrho_{\text{L}} + P_{\text{cov,N}}(\lambda, T, \nu)\, \varrho_{\text{N}}, \tag{20}$$

where $\varrho_{\text{L}} = 1 - \varrho_{\text{N}}$ is defined in Lemma 2, and $P_{\text{cov,L}}(\cdot)$ gives the conditional SINR coverage
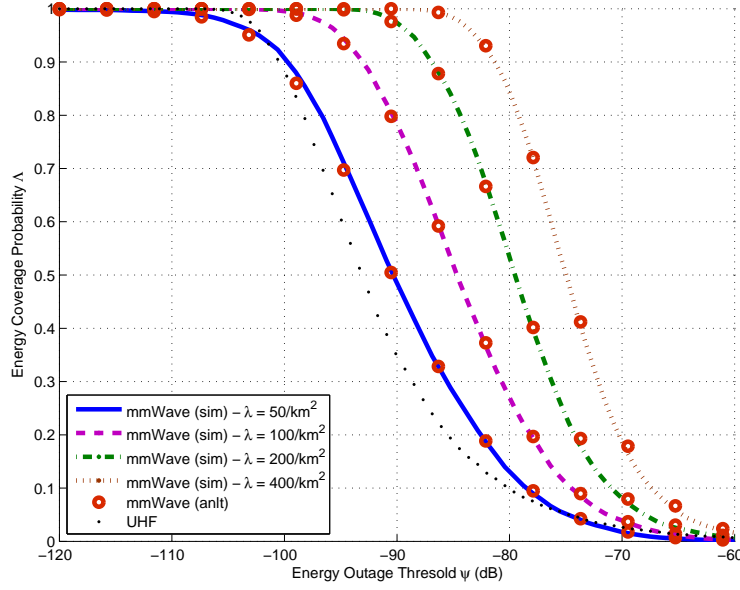
Fig. 6. Energy coverage probability $\Lambda(0, \psi, \lambda)$ for different network densities for nonconnected users. Transmit beam pattern is fixed to $[10, -10, 30°, 330°]$. Other parameters are same as given in Fig. 2. Monte Carlo simulation (sim) results validate the analytical (anlt) results obtained using Theorem 2 with $N = 5$ terms.

probability given the receiver is served by a LOS BS, and can be approximated as

$$
P_{\text{cov,L}}(\lambda, T, \nu) \approx \sum_{k=1}^{N_{\text{L}}} (-1)^{k+1} \binom{N_{\text{L}}}{k} \int_{r_g}^{\infty} e^{-\frac{k c_{\text{L}} r^{\alpha_{\text{L}}} T \left(\sigma^2 + \nu^{-1} \sigma_c^2\right)}{P C_{\text{L}} M_{\text{t}} M_{\text{r}}}} e^{-\Delta_{k,1}(T,r) - \Delta_{k,2}(T,r)} \tilde{\tau}_{\text{L}}(r) \, dr. \quad (21)
$$

Similarly, the conditional SINR coverage probability for the NLOS case $P_{\text{cov,N}}(\cdot)$ is given by

$$
P_{\text{cov,N}}(\lambda, T, \nu) \approx \sum_{k=1}^{N_{\text{N}}} (-1)^{k+1} \binom{N_{\text{N}}}{k} \int_{r_g}^{\infty} e^{-\frac{k c_{\text{N}} r^{\alpha_{\text{N}}} T \left(\sigma^2 + \nu^{-1} \sigma_c^2\right)}{P C_{\text{N}} M_{\text{t}} M_{\text{r}}}} e^{-\Delta_{k,3}(T,r) - \Delta_{k,4}(T,r)} \tilde{\tau}_{\text{N}}(r) \, dr, \quad (22)
$$

where

$$
\Delta_{k,1}(T, x) = 2\pi\lambda \sum_{i=1}^{4} p_i \int_{x}^{\infty} \left(1 - \left[1 + \frac{c_{\text{L}} k \tilde{D}_i T x^{\alpha_{\text{L}}}}{N_{\text{L}} t^{\alpha_{\text{L}}}}\right]^{-N_{\text{L}}}\right) p(t) t \, dt, \quad (23)
$$

$$
\Delta_{k,2}(T, x) = 2\pi\lambda \sum_{i=1}^{4} p_i \int_{\rho_{\text{L}}(x)}^{\infty} \left(1 - \left[1 + \frac{c_{\text{L}} k \tilde{D}_i C_{\text{N}} T x^{\alpha_{\text{L}}}}{N_{\text{N}} C_{\text{L}} t^{\alpha_{\text{N}}}}\right]^{-N_{\text{N}}}\right) (1 - p(t)) t \, dt, \quad (24)
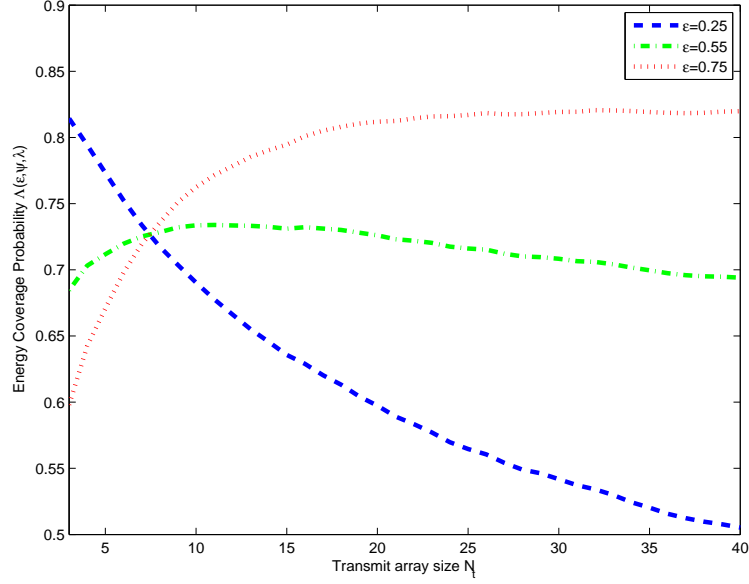$$

Fig. 7. The overall energy coverage probability $\Lambda(\epsilon, \psi, \lambda)$ for different values of $\epsilon$. Depending on the fraction of users operating in connected/nonconnnected modes, the transmit array size (which controls the beamforming beamwidth in this example) can be optimized to maximize the network-wide energy coverage. This could translate into massive gains given that the number of served devices would be potentially large. The users are assumed to be equipped with a single omnidirectional receive antenna. The energy outage threshold $\psi$ is $-70$ dB for $\Phi_{u,\text{con}}$ and $-85$ dB for $\Phi_{u,\text{ncon}}$. $P_{\text{t}} = 13$ dB, $\lambda = 200/\text{km}^2$. Channel parameters are same as used in Fig. 2.

$$\Delta_{k,3}(T, x) = 2\pi\lambda \sum_{i=1}^{4} p_i \int_{\rho_{\text{N}}(x)}^{\infty} \left( 1 - \left[ 1 + \frac{c_{\text{N}} k \tilde{D}_i C_{\text{L}} T x^{\alpha_{\text{N}}}}{N_{\text{L}} C_{\text{N}} t^{\alpha_{\text{L}}}} \right]^{-N_{\text{L}}} \right) p(t) t \mathrm{d}t, \tag{25}$$

$$\Delta_{k,4}(T, x) = 2\pi\lambda \sum_{i=1}^{4} p_i \int_{x}^{\infty} \left( 1 - \left[ 1 + \frac{c_{\text{N}} k \tilde{D}_i T x^{\alpha_{\text{N}}}}{N_{\text{N}} t^{\alpha_{\text{N}}}} \right]^{-N_{\text{N}}} \right) (1 - p(t)) t \mathrm{d}t, \tag{26}$$

$\tilde{D}_i = \frac{D_i}{M_{\text{t}} M_{\text{r}}}$ for $i \in \{1, 2, 3, 4, 5\}$, $c_{\text{L}} = N_{\text{L}} (N_{\text{L}}!)^{-\frac{1}{N_{\text{L}}}}$ and $c_{\text{N}} = N_{\text{N}} (N_{\text{N}}!)^{-\frac{1}{N_{\text{N}}}}$.

The following theorem provides the main result of this section.

*Theorem 3:* In a mmWave network of density $\lambda$, the success probability $P_{\text{suc}}(\lambda, T, \psi, \nu)$ given the SINR outage threshold $T$, the energy outage threshold $\psi$, and the power splitting ratio $\nu$ is given by

$$P_{\text{suc}}(\lambda, T, \psi, \nu) = P_{\text{cov}}(\lambda, T, \nu) \tilde{P}_{\text{con}}(\lambda, \mu) + P_{\text{con}}(\lambda, \varphi) \left[ 1 - \tilde{P}_{\text{con}}(\lambda, \mu) \right] \tag{27}$$

where the SINR coverage probability $P_{\text{cov}}(\cdot)$ can be evaluated using the expressions in Lemma

4, while the energy coverage probability $P_{\mathrm{con}}(\cdot)$ follows from Theorem 1. We further define $\tilde{P}_{\mathrm{con}}(\lambda, \mu) = \tilde{P}_{\mathrm{con,L}}(\lambda, \mu)\varrho_{\mathrm{L}} + \tilde{P}_{\mathrm{con,N}}(\lambda, \mu)\varrho_{\mathrm{N}}$, where $\tilde{P}_{\mathrm{con,L}}(\cdot)$ and $\tilde{P}_{\mathrm{ncon,N}}(\cdot)$ can be specified by (9) and (10) respectively with $\zeta_k^{\mathrm{L}}(\cdot) = \zeta_k^{\mathrm{N}}(\cdot) = 1$. Moreover, $\mu$ and $\varphi$ are a function of several parameters including the power splitting ratio $\nu$, the SINR outage threshold $T$, the energy outage threshold $\psi$, the rectifier efficiency $\xi$ as well as the noise parameters, and are given by

$$\mu = \frac{\psi}{\xi(1-\nu)(1+T)} - \sigma^2 - \frac{\sigma_c^2}{\nu(1+\frac{1}{T})}, \tag{28}$$

and $\varphi = \frac{\psi}{\xi(1-\nu)}$.

*Proof:* See Appendix D. ∎

Note that $\tilde{P}_{\mathrm{con}}(\lambda, \mu)$ in (27) is the interference CCDF evaluated at parameter $\mu$. It plays a key role in determining the operating mode of the system. Though the interference is harmful for information decoding, it can be beneficial for energy harvesting. When the interference is high, the SINR coverage probability will typically dominate the success probability. In the other extreme, the energy coverage probability will play the dominating role. Also note that the success probability can be optimized over the design paramter $\nu$, given other parameters. Moreover, we can recover the results in Theorem 1 and Lemma 4 from (27) by letting $\psi \to 0$ and $T \to 0$ respectively.

Note that, in principle, the success probability at a connected mmWave energy harvesting or SWIPT device can be further improved by leveraging large antenna arrays at the receiver, thanks to smaller wavelengths. Though our analytical model allows the users to have receive antenna arrays, it implicitly assumes the presence of ideal RF combining circuitry consisting of power-hungry components such as phase shifters, multiple RF chains, etc. When large antenna arrays are used at the receiver, the power consumption due to additional antenna circuitry may get prohibitively high, overshadowing the array gains. As SWIPT typically targets low-power devices, we present a simple low-power receiver architecture in the next section. Note that the analytical results based on Theorem 3 can be interpreted as an upper bound on performance when the receiver consists of suboptimal components (as is the case in the following section).

### B. Low-power Receiver Architecture

We now propose a novel architecture for a mmWave SWIPT receiver with multi-antenna array, as depicted in Fig. 8. In this architecture, we assume per-antenna power splitting with parameter
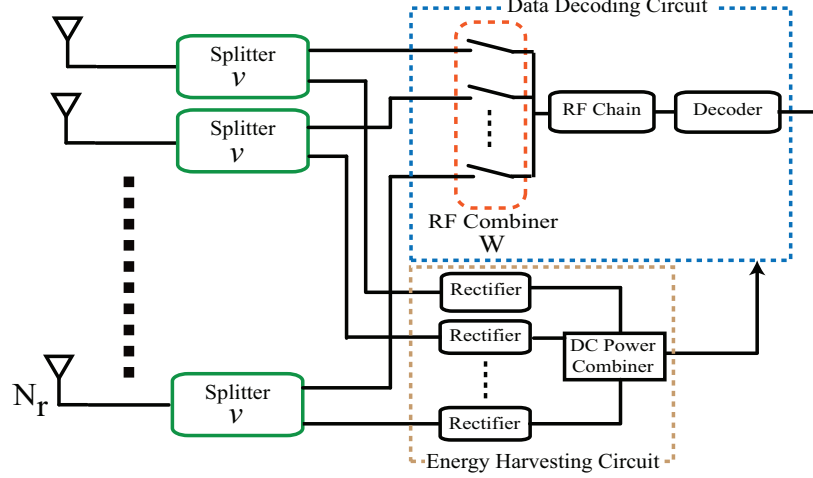
Fig. 8.  Low power receiver architecture for SWIPT.

$\nu$ (as defined earlier). After power splitting, the input signal at each antenna passes through a rectifier, followed by a DC combiner that yields the harvested energy. For the information path, after passing through power-splitters, the received signals are first combined in the RF domain using a combining vector $\mathbf{w}$. The resulting signal is then decoded in the baseband. Because they require extremely small power, the combining vector is assumed to be implemented using switches [28], i.e., $\mathbf{w} = [\mathbf{w}_1, \cdots, \mathbf{w}_{N_r}] \in [0, 1]^{N_r}$.

We now derive the combining gain expression for the proposed SWIPT receiver architecture in Fig. 8. Let $y$ be the signal output at the RF combiner. If a BS applies a beamforming vector $\mathbf{f} \in \mathbb{C}^{N_t \times 1}$ to send data symbol $s$ (where $\mathbb{E}\left[|s|^2\right] = P_t$) to a target user, it follows that

$$y = \sqrt{\nu}\left[\mathbf{w}^*\mathbf{H}_d\mathbf{f}s + \mathbf{w}^*\mathbf{r}_{\text{int}} + \mathbf{w}^*\mathbf{n}\right], \tag{29}$$

where $\mathbf{H}_d \in \mathbb{C}^{N_r \times N_t}$ is the channel between the user and its serving BS, and $\mathbf{r}_{\text{int}}$ is the received signal due to the interfering BSs. Since the channel between each user and its BS is assumed to be single-path, the channel matrix $\mathbf{H}_d = h_0\sqrt{g_0(r_0)}\mathbf{a}_r\left(\phi_r\right)\mathbf{a}_t\left(\phi_t\right)$, where $\mathbf{a}_t\left(\phi_t\right)$ and $\mathbf{a}_r\left(\phi_r\right)$ are the array response vectors at the BS and user, respectively. Recall that $g_o(r_o)$ denotes the path gain from the serving BS, while $\phi_r$ and $\phi_t$ respectively denote the channel angle of arrival and angle of departure at the user and BS. If the channel is known at the BS, and given the antenna model in Section II-C, the BS will design the beamforming vector $\mathbf{f}$ to maximize the beamforming gain, i.e., to have $\left|\mathbf{a}_t^*\left(\phi_t\right)\mathbf{f}\right|^2 = N_t$. Denoting $\bar{\alpha} = h_0\sqrt{g_0(r_0)}\mathbf{a}_t^*\left(\phi_t\right)\mathbf{f}$, the received

signal in (29) can be written as

$$y = \sqrt{\nu} \left( \bar{\alpha} \mathbf{w}^* \mathbf{a}_{\mathrm{r}} \left( \phi_{\mathrm{r}} \right) s + \mathbf{w}^* \mathbf{r}_{\mathrm{int}} + \mathbf{w}^* \mathbf{n} \right). \tag{30}$$

The post-combining SINR can then be expressed as

$$\mathrm{SINR} = \frac{\nu P_{\mathrm{t}} \left| \alpha \right|^2 N_t \left| \mathbf{w}^* \mathbf{a}_{\mathrm{r}} \left( \phi_{\mathrm{r}} \right) \right|^2}{I + \nu \mathbf{w}^* \mathbf{w} \sigma^2}, \tag{31}$$

where $\left| \mathbf{w}^* \mathbf{a}_{\mathrm{r}} \left( \phi_{\mathrm{r}} \right) \right|^2$ represents the combining gain at the receiver, and $I$ denotes the aggregate interference power. The SINR in (31) can be maximized if the receiver designs the optimum combining vector, which can be implemented by activating certain antennas on or off. This requires the receiver to have global channel knowledge, which is often challenging in practice. We relax this condition by assuming that the receiver has the angle of arrival information for the serving BS only. Ignoring the interference, we propose to design the combining vector by maximizing the $\mathrm{SNR} = \frac{P_{\mathrm{t}} |\bar{\alpha}|^2 N_t \left| \mathbf{w}^* \mathbf{a}_{\mathrm{r}} \left( \phi_{\phi_{\mathrm{r}}} \right) \right|^2}{\mathbf{w}^* \mathbf{w} \sigma^2}$ instead, i.e., the receiver designs its combining vector $\mathbf{w}$ such that

$$\mathbf{w}^{\star} = \arg \max_{\mathbf{w} \in [0,1]^{N_{\mathrm{r}}}} \frac{\left| \mathbf{w}^* \mathbf{a}_{\mathrm{r}} \left( \phi_{\mathrm{r}} \right) \right|^2}{\mathbf{w}^* \mathbf{w}}. \tag{32}$$

The optimal solution in (32) can be found by an exhaustive search over all possible combinations of $\mathbf{w}$. For large receive antenna arrays, this could entail high computational costs, which would further increase the power consumption. Therefore, it is important to consider computationally efficient approaches for designing the combining vector. As outlined in Algorithm 1, we propose a greedy solution for designing $\mathbf{w}$ by (step-wise) activating only those antennas that boost the received SNR. With $\hat{\mathbf{w}}$ denoting the combining vector designed using Algorithm 1, the combining gain for the switch-based architecture can be defined as $M_c = \frac{\left| \sum_{i=1}^{N_r} \hat{w}_i e^{\jmath k d (i-1) \cos(\phi_{\mathrm{r}})} \right|^2}{|\hat{\mathbf{w}}|^2}$ where $k$ denotes the wavenumber and $d$ is the antenna element spacing. Despite its low-complexity, numerical simulations in the next section reveal that our low-power greedy approach could give a good combining gain, without losing substantial performance compared to more advanced but power-hungry solutions.

---

**Algorithm 1** Greedy Switch Combining Design

---
**Input** $N_r$, $\phi_r$
**Initialization** $\mathbf{w} = 0$, $\mathbf{w}_1 = 1$
**for** $i = 2, \cdots, N_r$ **do**
    **if** $\frac{1}{i}\left|\sum_{n=1}^{i-1} \mathbf{w}_n e^{\mathrm{j}kd(n-1)\cos(\phi_r)} + e^{\mathrm{j}kd(i-1)\cos(\phi_r)}\right|^2 > \frac{1}{i-1}\left|\sum_{n=1}^{i-1} \mathbf{w}_n e^{\mathrm{j}kd(n-1)\cos(\phi_r)}\right|^2$ **then**
        $\mathbf{w}_i = 1$
    **end if**
**end for**

---

*C. Results*

Using Theorem 3, Fig. 9 plots the overall success probability for a given transmit antenna beam pattern. The users are equipped with a single-antenna receiver, similar to the one in Fig. 8 with $N_r = 1$. First, Fig. 9 shows that a good success probability can be obtained with mmWave SWIPT system for typical mmWave propagation and system parameters. Further, this plot illustrates that the power splitting ratio $\nu$ needs to be optimized for a given SINR outage threshold to maximize the overall success probability. Matching the intuition, the figure shows that in the low SINR outage regime (when $T$ is large), it is desirable to divert more power to the information decoding module, while a larger fraction of power needs to be portioned for the energy harvesting system in the high SINR outage regime (when $T$ is small). This trend is consistent with prior studies on SWIPT architectures [10].

We now evaluate the performance of the proposed low-power receiver architecture for different number of receive antennas. In Fig. 10, the success probability $P_{\mathrm{suc}}(\lambda, T, \psi, \nu)$ is plotted for a fixed transmit antenna beam pattern. For the proposed architecture, the combining vector is obtained using Algorithm 1, and the curves are averaged over the angle of arrival parameter. For comparison, we also plot the success probability for (fully digital) maximal ratio combining (MRC) receivers. We observe that the success probability improves with the receive antenna array size. Further, when the SINR outage threshold $T$ is small, the success probability is mainly limited by the energy outage. This also explains why the success probability converges to a limit (determined by the energy outage threshold) as $T$ decreases. Moreover, there are diminishing returns as the number of antennas are increased. A comparison with power-hungry MRC receivers shows that the proposed switch-based architecture performs reasonably well. This is particularly desirable for future mmWave SWIPT devices.
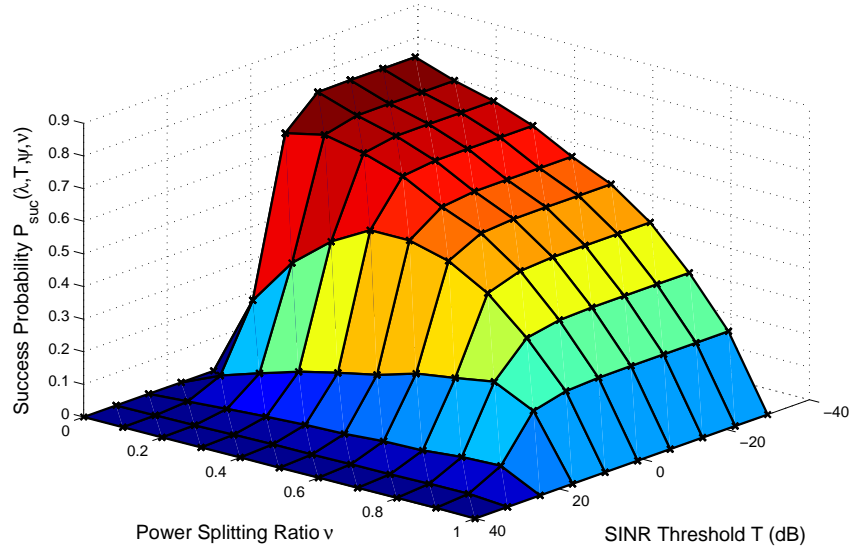
Fig. 9. A 3D plot showing the interplay between the success probability, the power splitting ratio $\nu$, and the SINR outage threshold $T$ for a given energy outage threshold $\psi$ and network density $\lambda$. As $T$ gets large, the system becomes SINR-limited, and the optimum value of $\nu$ increases, suggesting that a larger fraction of received signal should be used for information extraction to optimize the overall success probability. The transmit antenna beam pattern is set to $A_{15,-15,10^\circ,350^\circ}$. Other parameters include $\psi = -70$ dB, $\sigma_c^2 = -80$ dB, $\lambda = 200/\text{km}^2$, and $P_t = 43$ dBm.

## V. CONCLUSION

In this paper, we analyzed the energy harvesting performance at low-power devices powered by a mmWave cellular network. Using a stochastic geometry framework, we derived analytical expressions characterizing the performance of mmWave energy and information transfer in terms of system, channel and network parameters. Simulations results were used to validate the accuracy of the derived expressions. Leveraging the analytical framework, we also provided useful network and device level design insights. For the connected case when the transmitter and receiver beams are aligned, results show that the energy coverage improves with narrower beams. In contrast, wider beams provide better energy coverage when the receivers are not aligned with a particular transmitter. This trade-off is evident in the more general scenario having both types of receivers, where there typically exists an optimal beamforming beamwidth that maximizes the network-wide energy coverage. Moreover, we found that several device-related parameters can significantly impact the system performance. For example, the performance can be substantially improved by optimizing over the power splitting ratio and by leveraging large antenna arrays. To
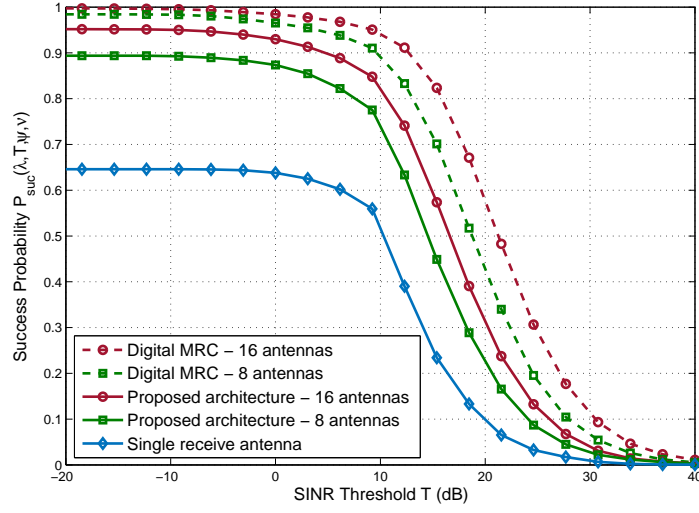
Fig. 10. The success probability for different number of receive antennas $N_{\mathrm{r}}$ at the user given a fixed transmit beam pattern $A_{15,-15,10°,350°}$ at the BSs. Proposed low-power architecture achieves good performance compared to superior receiver architectures. Other parameters include $\nu = 0.5$, $\psi = -70$ dB, $\sigma_c^2 = -80$ dB, $\lambda = 200/\text{km}^2$, and $P_{\mathrm{t}} = 43$ dBm.

allow using multiple antennas at the mmWave receivers while keeping the power consumption low, we proposed a low-power receiver architecture for mmWave energy and information transfer using antenna switches. Simulation results show that the proposed architecture can provide good gains for the overall mmWave energy harvesting performance. Simulation results also reveal that mmWave cellular networks could potentially provide better energy coverage than lower frequency solutions.

## APPENDIX A

The following inequality approximates the tail probability of a normalized Gamma distribution.

*Lemma 5 (From [29]):* For a normalized Gamma random variable $u$ with parameter $N$, the probability $\Pr(u < x)$ can be tightly upper-bounded by

$$\Pr(u < x) < \left(1 - e^{-ax}\right)^N$$

where the constant $x > 0$ and $a = N(N!)^{-\frac{1}{N}}$.

We write $\mathrm{P}_{\mathrm{con}}(\lambda, \psi) = \Pr[\gamma > \psi] = \Pr[S + I + \sigma^2 > \psi]$, where $S = P_{\mathrm{t}} M_{\mathrm{t}} M_{\mathrm{r}} H_0 g_0(r_0)$ and $I = \sum_{\ell > 0, \ell \in \Phi(\lambda) \backslash \mathbb{B}(r_g)} P_{\mathrm{t}} \delta_\ell H_\ell g_\ell(r_\ell)$. We can derive the result in Theorem 1 by finding the conditional

distributions $P_{con,L}(\lambda, \psi)$ and $P_{con,N}(\lambda, \psi)$. To proceed, first consider the conditional distribution $P_{con,L}(\lambda, \psi) = \Pr(S + I > \psi | L)$ given the receiver is aligned with a LOS BS (which is indicated by the subscript L in the following notation).

$$P_{con,L}(\lambda, \psi) = \mathbb{E}_{S,I|L}\left[\Pr\left(u < \frac{S+I}{\psi}\right)\right] \overset{(a)}{\approx} \mathbb{E}_{S,I|L}\left[\left(1 - e^{-a\frac{S+I}{\psi}}\right)^N\right]$$

$$= \mathbb{E}_{S,I|L}\left[\sum_{k=0}^{N}(-1)^k \binom{N}{k} e^{-ak\frac{S+I}{\psi}}\right] = \sum_{k=0}^{N}(-1)^k \binom{N}{k}\mathbb{E}_{S,I|L}\left[e^{-\hat{a}(S+I)}\right] \qquad (33)$$

where we have included a dummy random variable $u \sim \Gamma\left(N, \frac{1}{N}\right)$ in the first equation. Note that $u$ converges to 1 as $N \to \infty$. Therefore, this substitution is in fact an approximation when $N$ is finite. The introduction of $u$ allows leveraging the inequality in Lemma 4, which leads to $(a)$, where the constant $a = N(N!)^{-\frac{1}{N}}$. The last equation follows from the Binomial series expansion of $(b)$, and by further substituting $\hat{a} = \frac{ak}{\psi}$. To evaluate the expectation in (33), consider

$$\mathbb{E}_{S,I|L}\left[e^{-\hat{a}(S+I)}\right] = \mathbb{E}_{S|L}\left[e^{-\hat{a}S}\mathbb{E}_{I|S,L}\left[e^{-\hat{a}I}\right]\right]. \qquad (34)$$

The inner expectation in (34) can be simplified by applying the thinning theorem for a PPP [24]. Note that $\Phi$ can be independently thinned into two PPPs $\Phi_L$ and $\Phi_N$, where the former comprises the LOS BSs whereas the latter consists of NLOS BSs. We can further thin $\Phi_L$ into four independent PPPs $\{\Phi_L^i\}_{i=1}^4$, where each resulting PPP $\Phi_L^i$ contains BSs that correspond to a nonzero directivity gain $D_i$ with $p_i$ being the thinning probability. This follows because the beam orientations are assumed to be independent across links. Thus, a link can have a directivity gain of $D_i$ with probability $p_i$ independently of other links. We let the received power due to the transmission from the BSs in $\Phi_L^i$ be $I_L^i$. Likewise, $\Phi_N$ can be split into $\{\Phi_N^i\}_{i=1}^4$ with the corresponding received powers denoted by $\{I_N^i\}_{i=1}^4$. Since the resulting PPPs are independent, (34) can be simplified as

$$\mathbb{E}_{I|S,L}\left[e^{-\hat{a}I}\right] = \prod_{i=1}^{4}\mathbb{E}_{I|S,L}\left[e^{-\hat{a}I_L^i}\right]\prod_{j=1}^{4}\mathbb{E}_{I|S,L}\left[e^{-\hat{a}I_N^j}\right] \qquad (35)$$

where $\mathbb{E}_{I|S,\mathrm{L}}\left[e^{-\hat{a}I_\mathrm{L}^i}\right]$ equals

$$
\mathbb{E}_{\Phi_\mathrm{L}^i,H|r_o}\left[e^{-\hat{a}\sum\limits_{\ell\in\Phi_\mathrm{L}^i\backslash\mathbb{B}(r_o)}P_\mathrm{t}H_\ell D_i C_\mathrm{L}r_\ell^{-\alpha_\mathrm{L}}}\right]\overset{(a)}{=}\mathbb{E}_{\Phi_\mathrm{L}^i|r_o}\left[\prod_{\ell\in\Phi_\mathrm{L}^i\backslash\mathbb{B}(r_o)}\mathbb{E}_{H_\ell}\left[e^{-\hat{a}P_\mathrm{t}H_\ell D_i C_\mathrm{L}r_\ell^{-\alpha_\mathrm{L}}}\right]\right]
$$

$$
\overset{(b)}{=}\mathbb{E}_{\Phi_\mathrm{L}^i|r_o}\left[\prod_{\ell\in\Phi_\mathrm{L}^i\backslash\mathbb{B}(r_o)}\left(\frac{1}{1+\hat{a}P_\mathrm{t}D_i C_\mathrm{L}r_\ell^{-\alpha_\mathrm{L}}N_\mathrm{L}^{-1}}\right)^{N_\mathrm{L}}\right]=e^{-2\pi\lambda p_i\int\limits_{r_o}^{\infty}\left(1-\left(\frac{1}{1+\hat{a}P_\mathrm{t}D_i C_\mathrm{L}t^{-\alpha_\mathrm{L}}N_\mathrm{L}^{-1}}\right)^{N_\mathrm{L}}\right)p(t)t\mathrm{d}t}
$$

(36)

where $(a)$ follows by conditioning on the length $r_o$ of the serving LOS link, and by further noting that small-scale fading is independent across links. Here, $\mathbb{B}(r_o)$ denotes a circular disc of radius $r_o$ centered at the typical user. $(b)$ is obtained by using the moment generating function of a normalized Gamma random variable, while the last equation follows by invoking the probability generating functional [24] of the PPP $\Phi_L^i$. Substituting (36) in the first (left) product term of (35) yields (11). Similarly, $\mathbb{E}_{I|S,\mathrm{L}}\left[e^{-\hat{a}I_\mathrm{N}^i}\right]$ is given by

$$
\mathbb{E}_{\Phi_\mathrm{L}^i,H|r_o}\left[e^{-\hat{a}\sum\limits_{\ell\in\Phi_\mathrm{N}^i\backslash\mathbb{B}(\rho_\mathrm{L}(r_o))}P_\mathrm{t}H_\ell D_i C_\mathrm{N}r_\ell^{-\alpha_\mathrm{N}}}\right]=e^{-2\pi\lambda p_i\int\limits_{\rho_\mathrm{L}(r_o)}^{\infty}\left(1-\left(\frac{1}{1+\hat{a}P_\mathrm{t}D_i C_\mathrm{N}x^{-\alpha_\mathrm{N}}N_\mathrm{N}^{-1}}\right)^{N_\mathrm{N}}\right)(1-p(t))t\mathrm{d}t}.
$$

(37)

By substituting (37) in the second (right) product term of (35) yields (12). Using the expressions in (35)–(37) in (34), and by further evaluating the expectation of the resulting expression with respect to $S$, we obtain

$$
\int\limits_{r_g}^{\infty}\left(\frac{1}{1+\hat{a}P_\mathrm{t}M_\mathrm{t}M_\mathrm{r}C_\mathrm{L}r^{-\alpha_\mathrm{L}}N_\mathrm{L}^{-1}}\right)^{N_\mathrm{L}}e^{-\Upsilon_{k,1}(\lambda,\psi,r)-\Upsilon_{k,2}(\lambda,\psi,\rho_\mathrm{L}(r))}\times\tilde{\tau}_\mathrm{L}(r)\mathrm{d}r
$$

(38)

where we have again used definition of the moment generating function of a normalized Gamma distribution. $\Upsilon_{k,1}(\cdot)$ and $\Upsilon_{k,2}(\cdot)$ are given in (11) and (12) respectively, $r_g$ denotes the minimum link distance, while the distance distribution is provided in Lemma 3. Using (33) and (34), we can thus retrieve the expression in (9). We can similarly derive the conditional distribution $\mathrm{P}_{\mathrm{con,N}}(\lambda,\psi)=\mathrm{Pr}(S+I>\psi|\mathrm{N})$ in (10) for the NLOS case.

## APPENDIX B: PROPOSITION 1

We can derive Proposition 1 by finding the conditional means $\bar{P}_{\mathrm{L}} = \mathbb{E}\left[S + I|\mathrm{L}\right]$ and $\bar{P}_{\mathrm{N}} = \mathbb{E}\left[S + I|\mathrm{N}\right]$. $\bar{P}_{\mathrm{L}}$ can be evaluated by conditioning on the link distance $r_0$ from the serving BS as follows.

$$\mathbb{E}\left[S + I|r_0, \mathrm{L}\right] = \mathbb{E}\left[S|r_0, \mathrm{L}\right] + \sum_{i=1}^{4}\mathbb{E}\left[I_{\mathrm{L}}^i + I_{\mathrm{N}}^i|r_0, \mathrm{L}\right]$$

$$\stackrel{(a)}{=} P_{\mathrm{t}}M_{\mathrm{t}}M_{\mathrm{r}}C_{\mathrm{L}}{r_0}^{-\alpha_{\mathrm{L}}} + \sum_{i=1}^{4}2\pi\lambda P_{\mathrm{t}}p_i D_i C_{\mathrm{L}}\int_{r_0}^{\infty} t^{-(\alpha_{\mathrm{L}}-1)}p(t)\mathrm{d}t +$$

$$\sum_{i=1}^{4}2\pi\lambda P_{\mathrm{t}}p_i D_i C_{\mathrm{N}}\left[\frac{(\rho_{\mathrm{L}}(r_0))^{-(\alpha_{\mathrm{N}}-2)}}{\alpha_{\mathrm{N}} - 2} - \int_{\rho_{\mathrm{L}}(r_0)}^{\infty} t^{-(\alpha_{\mathrm{N}}-1)}p(t)\mathrm{d}t\right]$$

$$= P_{\mathrm{t}}M_{\mathrm{t}}M_{\mathrm{r}}C_{\mathrm{L}}{r_0}^{-\alpha_{\mathrm{L}}} + \Psi_{\mathrm{L}}\left(r_0\right) + \Psi_{\mathrm{N}}\left(\rho_{\mathrm{L}}(r_0)\right) \tag{39}$$

where $(a)$ is obtained by averaging over the fading distribution, followed by invoking Campbell's theorem [24], while (39) follows from the definitions of $\Psi_{\mathrm{L}}$ and $\Psi_{\mathrm{N}}$ provided in (16) and (17) respectively. Taking expectation of $\mathbb{E}\left[S + I|r_0, \mathrm{L}\right]$ with respect to $r_o$ using Lemma 3 yields (14). The expression for $\bar{P}_{\mathrm{N}}$ is (15) can be derived using similar steps.

## APPENDIX C: THEOREM 2

We now derive an analytical approximation for the energy coverage probability $\mathrm{P}_{\mathrm{ncon}}\left(\lambda, \psi\right) = \mathrm{Pr}\{\gamma > \psi\}$ in the nonconnected case. Since no prior beam alignment is assumed for this case, the directivity gain $\delta_\ell$ would be random for any BS $\ell \in \Phi$. We therefore let $\gamma = I + \sigma^2$ where $I = \sum_{\ell \in \Phi(\lambda)\backslash\mathbb{B}(r_g)} P_{\mathrm{t}}\delta_\ell H_\ell g_\ell(r_\ell)$ and $r_g$ defines the minimum link distance. Using the steps similar to those in (33), (36) and (37), it follows that $\mathrm{P}_{\mathrm{ncon}}\left(\lambda, \psi\right) =$

$$\mathrm{Pr}\left(1 < \frac{I}{\hat{\psi}}\right) = \mathbb{E}_I\left[\sum_{k=0}^{N}(-1)^k\binom{N}{k}e^{-\frac{ak}{\hat{\psi}}I}\right] = \sum_{k=0}^{N}(-1)^k\binom{N}{k}e^{-\Upsilon_{k,1}\left(\lambda,\hat{\psi},r_g\right)-\Upsilon_{k,2}\left(\lambda,\hat{\psi},r_g\right)} \tag{40}$$

where $\hat{\psi} = \psi - \sigma^2$, while $\Upsilon_{k,1}(\cdot)$ and $\Upsilon_{k,2}(\cdot)$ follow from (11) and (12) respectively.

## APPENDIX D: THEOREM 3

We proceed by recalling that $\gamma = (1 - \nu)\left(S + I + \sigma^2\right)$ where $S = P_{\mathrm{t}} M_{\mathrm{t}} M_{\mathrm{r}} H_0 g_0(r_0)$ and $I = \sum_{\ell > 0, \ell \in \Phi(\lambda) \backslash \mathbb{B}(r_g)} P_{\mathrm{t}} \delta_\ell H_\ell g_\ell(r_\ell)$. To find $P_{\mathrm{suc}}\left(\lambda, T, \psi, \nu\right) = \Pr\left[\mathrm{SINR} > T, \gamma > \psi\right]$, consider

$$
\Pr\left[\frac{\nu S}{\nu(I + \sigma^2) + \sigma_c^2} > T, (1 - \nu)\left(S + I + \sigma^2\right) > \psi\right]
$$

$$
= \mathbb{E}_I\left[\Pr\left[S > T\left(I + \sigma^2 + \frac{\sigma_c^2}{\nu}\right), S > \frac{\psi}{1 - \nu} - I - \sigma^2\right]\right]
$$

$$
\overset{(a)}{=} \mathbb{E}_I\left[\Pr\left[S > T\left(I + \sigma^2 + \frac{\sigma_c^2}{\nu}\right)\right]\right]\Pr\left[I > \mu\right] + \mathbb{E}_I\left[\Pr\left[S > \frac{\psi}{1 - \nu} - I - \sigma^2\right]\right]\Pr\left[I \leq \mu\right]
$$

$$
= P_{\mathrm{cov}}(\lambda, T, \nu)\tilde{P}_{\mathrm{con}}(\lambda, \mu) + P_{\mathrm{con}}(\lambda, \varphi)\left[1 - \tilde{P}_{\mathrm{con}}(\lambda, \mu)\right] \tag{41}
$$

where the SINR coverage probability $P_{\mathrm{cov}}(\lambda, T, \nu)$ follows from Lemma 4, and the energy coverage probability $P_{\mathrm{con}}(\lambda, \varphi)$ from Theorem 1. $\tilde{P}_{\mathrm{con}}(\lambda, \mu)$ is the interference CCDF evaluated at $\mu$, where $\mu$ given in (28) follows from the inequality $T\left(I + \sigma^2 + \frac{\sigma_c^2}{\nu}\right) > \frac{\psi}{1 - \nu} - I - \sigma^2$.

## REFERENCES

[1] T. S. Rappaport, R. W. Heath Jr, R. C. Daniels, and J. N. Murdock, *Millimeter Wave Wireless Communications*. Pearson Education, 2014.

[2] T. Bai, A. Alkhateeb, and R. Heath, "Coverage and capacity of millimeter-wave cellular networks," *IEEE Commun. Mag.*, vol. 52, pp. 70–77, Sept. 2014.

[3] S. Ulukus, A. Yener, E. Erkip, O. Simeone, M. Zorzi, P. Grover, and K. Huang, "Energy harvesting wireless communications: A review of recent advances," *IEEE J. Sel. Areas Commun.*, vol. 33, pp. 360–381, Mar. 2015.

[4] A. Zanella, N. Bui, A. Castellani, L. Vangelista, and M. Zorzi, "Internet of things for smart cities," *IEEE Internet Things J.*, vol. 1, pp. 22–32, Feb. 2014.

[5] S. Rangan, T. S. Rappaport, and E. Erkip, "Millimeter wave cellular wireless networks: Potentials and challenges," *arXiv preprint arXiv:1401.2560*, 2014.

[6] V. Talla, B. Kellogg, B. Ransford, S. Naderiparizi, S. Gollakota, and J. R. Smith, "Powering the next billion devices with Wi-Fi," *arXiv preprint arXiv:1505.06815*, 2015.

[7] S. Gollakota, M. Reynolds, J. Smith, and D. Wetherall, "The emergence of RF-powered computing," *Computer*, vol. 47, pp. 32–39, Jan. 2014.

[8] M. Pinuela, P. Mitcheson, and S. Lucyszyn, "Ambient RF energy harvesting in urban and semi-urban environments," *IEEE Trans. Microw. Theory Techn.*, vol. 61, pp. 2715–2726, Jul. 2013.

[9] C. Valenta and G. Durgin, "Harvesting wireless power: Survey of energy-harvester conversion efficiency in far-field, wireless power transfer systems," *IEEE Microw. Mag.*, vol. 15, pp. 108–120, Jun. 2014.

[10] S. Bi, C. Ho, and R. Zhang, "Wireless powered communication: opportunities and challenges," *IEEE Commun. Mag.*, vol. 53, pp. 117–125, Apr. 2015.

[11] R. Zhang and C. K. Ho, "MIMO broadcasting for simultaneous wireless information and power transfer," *IEEE Trans. Wireless Commun.*, vol. 12, pp. 1989–2001, May 2013.

[12] L. Liu, R. Zhang, and K.-C. Chua, "Wireless information transfer with opportunistic energy harvesting," *IEEE Trans. Wireless Commun.*, vol. 12, pp. 288–300, Jan. 2013.

[13] J. Park and B. Clerckx, "Joint wireless information and energy transfer in a two-user MIMO interference channel," *IEEE Trans. Wireless Commun.*, vol. 12, pp. 4210–4221, Aug. 2013.

[14] I. Flint, L. Xiao, N. Privault, D. Niyato, and P. Wang, "Performance analysis of ambient RF energy harvesting with repulsive point process modeling," *IEEE Trans. Wireless Commun.*, vol. PP, no. 99, pp. 1–1, 2015.

[15] S. Lee, R. Zhang, and K. Huang, "Opportunistic wireless energy harvesting in cognitive radio networks," *IEEE Trans. Wireless Commun.*, vol. 12, pp. 4788–4799, Sep. 2013.

[16] A. Sakr and E. Hossain, "Cognitive and energy harvesting-based D2D communication in cellular networks: Stochastic geometry modeling and analysis," *IEEE Trans. Commun.*, vol. 63, pp. 1867–1880, May 2015.

[17] K. Huang and V. Lau, "Enabling wireless power transfer in cellular networks: Architecture, modeling and deployment," *IEEE Trans. Wireless Commun.*, vol. 13, pp. 902–912, Feb. 2014.

[18] K. Huang and E. Larsson, "Simultaneous information and power transfer for broadband wireless systems," *IEEE Trans. Sig. Proc.*, vol. 61, pp. 5972–5986, Dec. 2013.

[19] I. Krikidis, "Simultaneous information and energy transfer in large-scale networks with/without relaying," *IEEE Trans. Commun.*, vol. 62, pp. 900–912, Mar. 2014.

[20] T. Bai and R. Heath, "Coverage and rate analysis for millimeter-wave cellular networks," *IEEE Trans. Wireless Commun.*, vol. 14, pp. 1100–1114, Feb. 2015.

[21] S. Singh, M. Kulkarni, A. Ghosh, and J. Andrews, "Tractable model for rate in self-backhauled millimeter wave cellular networks," *IEEE J. Sele. Areas Commun.*, vol. PP, no. 99, pp. 1–1, 2015.

[22] T. Bai, R. Vaze, and R. Heath, "Analysis of blockage effects on urban cellular networks," *IEEE Trans. Wireless Commun.*, vol. 13, pp. 5070–5083, Sep. 2014.

[23] A. Hunter, J. Andrews, and S. Weber, "Transmission capacity of ad hoc networks with spatial diversity," *IEEE Trans. Wireless Commun.*, vol. 7, pp. 5058–5071, Dec. 2008.

[24] M. Haenggi, *Stochastic geometry for wireless networks*. Cambridge University Press, 2012.

[25] T. Wu, T. S. Rappaport, and C. M. Collins, "The human body and millimeter-wave wireless communication systems: Interactions and implications," *arXiv preprint arXiv:1503.05944*, 2015.

[26] A. Ghosh, J. Zhang, J. G. Andrews, and R. Muhamed, *Fundamentals of LTE*. Pearson Education, 2010.

[27] H. L. Van Trees, *Detection, estimation, and modulation theory, optimum array processing*. John Wiley & Sons, 2004.

[28] R. Méndez-Rial, C. Rusu, A. Alkhateeb, N. González-Prelcic, and R. W. Heath Jr, "Channel estimation and hybrid combining for mmWave: Phase shifters or switches?," in *Inf. Theory and Applications Workshop (ITA)*, 2015.

[29] H. Alzer, "On some inequalities for the incomplete gamma function," *Mathematics of Computation of the American Mathematical Society*, vol. 66, no. 218, pp. 771–778, 1997.